ORIGINAL RESEARCH ARTICLE

The influence of atmospheric light scattering on reflectance measurements during photogrammetric survey flights at low altitudes over forest areas

Anna Mazur[1] iD**, Mariusz Kacprzak[1]** iD**, Katarzyna Kubiak[1,2], Jan Kotlarz[1]*** iD**, Krzysztof Skocki[1]**

[1]Institute of Aviation, Remote Sensing Division, al. Krakowska 110/114, 02–256 Warsaw, Poland; [2]Forest Research Institute, Department of Forest Protection, ul. Braci Leśnej 3, 05–090 Raszyn, Poland

*Tel. +48 22 8460011, ext. 835, e-mail: jan.kotlarz@ilot.edu.pl

Abstract. In this article, we describe methods for the correction of multispectral aerial images by accounting for atmospheric interference. We also summarize the first correction results for images acquired at flight altitudes and evaluate the suitability of selected methods for the atmospheric correction of these images. Furthermore, processes and phenomena occurring in the atmosphere that potentially affect image quality and interfere with the electromagnetic radiation registered by the imaging sensors are discussed as well. The purpose of atmospheric correction is to reduce or eliminate atmospheric interference during multispectral image processing. Here we present methodology for image correction based on data gathered at various altitudes during the autumn flights conducted as a part of the HESOFF project.

1. Introduction

Multispectral aerial and satellite images have a large interpretation potential. Information recorded in the form of radiometric pixel values is used to study the environment with particular reference to the status of water and vegetation, including analysis of trees, meadows and cereals. To carry out the quantitative and qualitative analysis, image data should be prepared appropriately. The relevant works include calibration of detectors, correction of the influence of the position of the Sun, topographical correction and atmospheric correction, the essence of which is the removal of the atmosphere impact on the values recorded in the image (Osińska-Skotak 2007, Ochtyra et al. 2016).

The necessity to carry out the atmospheric correction depends on picture purposes. Atmospheric correction is usually needless in the case of photographs taken to classify land cover or detect changes in time series. Simple atmospheric correction algorithms (including DOS) can be used in the absence of the need to obtain information about reflectance. If this parameter is necessary for conducting further analyses, more advanced algorithms ought to be used (Song 2001).

Currently, two chief methods can be applied in multispectral data calibration. The first includes the use of ready algorithms encrypted in the atmosphere models. Remote sensing software has special modules to eliminate the effects of the atmosphere. The most popular software packages with complicated models and algorithms are MODTRAN5 (2015), ATCOR2/3 and ATCOR4 (2015). Nonetheless, the obtained results are not always correct due to high dynamics of changes taking place in the atmosphere. The effectiveness of the procedure depends on the degree of correlation of the atmosphere model with its real state at the moment of obtaining images. The second group of methods is correction based on empirical data obtained directly in a given area. Field works consist of measurements with a spectrometer or the use of special calibration markers with known reflectance. The influence of the atmosphere is noticeable in qualitative analyses, including land cover classification, while it does not have a large impact on the obtained quantitative results (Osińska-Skotak 2005). In the case of quantitative analyses, even relatively small changes in values attributable to the passage of solar radiation through the atmosphere may be of key importance for the values of the calculated indicators and the results of the conducted research.

Figure 1. Calibration markers with (a) >95% and (b) <5% reflectance photographed from altitude 800 m

2. Atmospheric influence on pixel values in aerial and satellite images

The reflectance, registered as the value of a given pixel in an aerial/satellite image, is influenced by various processes taking place in the atmosphere. Considering radiation absorption and scattering is of much importance in further data processing. Making use of atmospheric corrections constitutes the initial stage of radiometric adjustments of multispectral images. The goal is to eliminate the effects of phenomena occurring in the atmosphere as completely as possible in relation to the measurement of reflectance (Osińska-Skotak 2007). Before calculating the remote sensing indices or conducting terrain classification, it is necessary to determine the effect of the atmosphere on the results. A particularly large error may be attributable to data from sensors placed on observation satellites, due to the thick atmosphere layer. The process of atmospheric correction applied to satellite images is complicated and requires mathematical and physicochemical modelling that takes into account the parameters of the atmosphere (Kotula 2011). Atmospheric correction methods have developed with the development of optical sensors. Their use on a large scale is associated with the acquisition of digital photos. Notwithstanding numerous studies carried out in order to fully describe the processes taking place in the atmosphere, there still remains the need to continue work, improve existing correction algorithms and develop techniques to study the instantaneous composition of compounds in consequence of electromagnetic radiation (Głowienka 2008). The air consists mainly of a mixture of gases (dry air), water in three phases and the atmospheric aerosol (Khodri 2017), that is, a suspension of solid and liquid particles (Wołoszyn 2009). The content of water vapor in the atmosphere varies, under-

goes phase transitions, depends on latitude, and its residence time in the atmosphere is estimated for about 10 days. The highest content of water vapor in the atmosphere is directly at the surface and decreases with the distance from the ground. At the height of 1.5 km, the average concentration of water vapor is 50% lower than at the Earth's surface, and at a height of 5 km, the water vapor content is 10 times lower, whereas at a height of 10 km, is it 100 times lower. The greatest part (about 99%) of water vapor is contained in the layer up to a height of 12 km (Wołoszyn 2009). Modelling the composition of the atmosphere is particularly difficult over the areas covered with vegetation. The gas exchange between the plants and the atmosphere is intense and depends on many factors (time of day, season of the year, outdoor lighting, etc.). In addition, the recorded reflectance and remote sensing indicators are influenced by the angles between the local vertical axis and the optical axis of the system recording the radiation, as well as the position of the Sun. This influence is visible three times more in the blue optical channels than those infrared. As a result, typical vegetation indices, such as the normalized difference vegetation index (NDVI), can be changed up to 50% (Burkat 2015). In data post-processing, the effects of reflectance geometry must be taken into account in addition to atmospheric correction.

The biosphere plays a key role in the global carbon cycle as plant green organs absorb carbon dioxide from the atmosphere and convert it to organic compounds with the contribution of solar energy (photosynthesis), while producing oxygen as a by-product in this process. In the respiration process, solar energy acquired in photosynthesis is stored in the form of organic chemical energy. Respiration (also indispensable process for plant growth) involves taking up oxygen and releasing CO_2 and also leads to a return of 60 petagrams of carbon/year (PgC/year) (Badawy 2011). Respiration plays an important role in the carbon balance at the plant cell, whole plant and ecosystem levels. Although the emission and absorption of CO_2, water vapor and oxygen plays a key role in their gas exchange, plants also produce and emit trace amounts of gases in a class called collectively biogenic volatile organic compounds (BVOCs). The emission of these can be an important part of the carbon balance in the forest ecosystem and can amount to about 1.3 PgC/year at a global level (Houghton 2017).

Vegetation is the main source of volatile organic compounds (VOCs) in the atmosphere. Direct plant emissions may include isoprenoids, terpenoids and various types of oxidized compounds (oVOC), such as aldehydes, organic acids, esters and alcohols. Many VOCs released have at least one olefinic bond in their chemical structure, making them very sensitive (reactive) to the oxidants present in the atmosphere (OH, O3, NO3), which ultimately oxidize VOC to CO_2. VOCs emit-

ted by plants are dominated by isoprene and its derivatives, such as monoterpenes and sesquiterpenes (Kiendler-Scharr et al. 2009). Unfortunately, knowledge about the temporal and spatial variability of BVOC emissions and their role in aerosol formation remains incomplete. BVOCs operate as ozone precursors, and thus, they indirectly absorb solar radiation in the ultraviolet range (Trainer et al., 1987). VOC emission from plants is limited by both physiological and physicochemical factors. Physiological factors affect the availability of BVOC precursors and enzymes that control their transformation. Physicochemical factors limiting BVOC emissions are: air parameters (temperature, partial-phase pressure, water and lipid phase concentration), gas diffusion, hydrophobic and hydrophilic properties of organic compounds inside the leaves, gas diffusion at the leaf and atmosphere border (Niinemets et al., 2004). The volume of BVOC emissions also depends on insolation intensity, CO_2 concentration in the atmosphere, plant genetic features, stage of leaf development and phenology. The volumes of VOC emissions depend on the plant species and can vary up to four orders of magnitude. Also, differences in biomass density and vegetation developmental stages affect emission volumes. BVOCs produced by forests impair visibility and can affect climate by scattering and absorbing solar radiation. Additionally, they can act as condensation nuclei and cause clouds to form. The main components of BVOCs are isoprene, monoterpenes, methanol, acetone, formaldehyde and acetaldehyde.

The composition of the atmosphere is variable over time and difficult to precisely model. It should be kept in mind that with airborne images taken at a relatively low altitude (< 2000 m), the atmosphere effect can be significant due to the fact that when compared to the model, half of the atmosphere mass is contained in the lower layer (merely 5000 m thick), which undergoes dynamic changes. Therefore, it is important to track atmosphere effects on the results obtained in processing of remote sensing data. Multispectral images obtained from low and medium altitudes (up to 2000 m) are less popular than relatively often used multispectral satellite imagery (Czapski et al. 2014), which is why, there have been considerably fewer scientific publications available, related to the radiometric correction for these areas. Based on the subject literature, we assumed that atmospheric correction can be made using two key methods: absolute and empirical, that is, relative (Głowienka 2008).

3. Methods for atmospheric correction

The absolute correction is performed based on the standard atmosphere models or on the basis of measurements of atmospheric parameters at the moment of image taking. The methods applied rely on the use of Radiative Transfer Model (RTM), based on the models of average climatic atmosphe-

res. This means that the current state of the atmosphere at the time of registration is not recorded, but the average state of the atmosphere in a specific climatic region. Radiation transfer models are physico-mathematical models describing the transmission of radiation in the atmosphere based on the laws of physics and effects of radiation on vegetation (Jarocińska 2012). The empirical (relative) correction method consists of comparing the terrestrial signal with another reference signal registered in the image. This method uses image and field measurements to perform the correction. It is based mainly on statistical measurements. The parameters can be obtained directly from the image, for example, with the use of Dark-Object-Subtraction (Kaneko 2016) Model (DOS), Flat Field (FF), Internal Average Relative Reflectance (IARR) or spectrometric field measurement, for example, by the Empirical Line method (Głowienka 2008).

The aim of the present study was to assess the impact of atmosphere on the radiometric values of objects recorded in aerial images, using the empirical method. An attempt was also made to answer the question whether it is possible to achieve satisfactory results in the calculation of NDVI, NDWI, RSI and other indices without correction, using images from the multi-spectral platform Quercus 6, created as part of the project HESOFF.

4. Materials and methods

For the correct analysis of the acquired multispectral images, it is necessary to properly prepare data and minimize the influence of factors interfering with the radiometric value. Correct data calibration is possible because of the use of field markers with the known reflection values in individual spectral ranges.

It was assumed that the markers used in the study must meet the basic parameters:
• possible low (< 20%) and possibly high (> 80%) spectral reflection in the ranges used to study trees; spectral reflection of the reference material must be predictable - irrespective of the position and light conditions
• Lambertian character reflectance/diffusion of the light
• appropriate terrain size of at least 3 x Ground Sampling Distance (GSD) cm (expected maximum pixel size); this is a limit value for effective detection (Campbell, Shin 2012, Tellidis, Levin 2014)

In order to calibrate the optical sensors from the plane, the Zenith Lite Target field markers were used from Sphere Optics (Figure 1) – 50 × 50 cm aluminium square sheets coated with a barium sulphate ($BaSO_4$) layer, and placed close to the forest area under investigation. Typical reflectance values for markers were below 5% (dark ones) and above 95% (light ones). Figure 3 shows the spectral curves for the

Figure 2. Low (<5%) and high (>95%) reflectance in visual and near infrared light calibration markers used in HESOFF project

markers. The use of field markers enabled correct calibration of the sensors and data processing that eliminated the atmosphere influence on reflectance depicted in the images, and, in particular, non-selective scattering on water vapour and VOC particles.

The comparison of the results obtained with the results of the selected atmospheric correction algorithms was made for a series of images made from various flight levels above the area of Żelechów, at the beginning of October 2014. A comparison with two correction algorithms, QUAC and FLAASH, was also performed in order to illustrate the problems related to the application of atmospheric correction in airborne images.

The QUAC algorithm is a typical "black box" algorithm, which takes into account the general atmosphere models and does not allow entering own parameters in the correction process, which significantly reduces its suitability for correcting aerial images taken at low flight heights, with a strong impact of local non-standard atmospheric components.

To obtain the correct result, the FLAASH algorithm requires input of many parameters characterizing the image obtained, as

well as environmental and meteorological conditions at the time of image taking. For the data obtained from typical photogrammetric flights, this can be difficult, more so that the algorithm for proper operation requires the use of an infrared channel (about 2 μm), which is not recorded in such air raids. This causes errors in the resulting images after correction (Figure 6).

The analysis of changeability of brightness intensity of selected pixels and image fragments was performed in the function of wavelength (channels) and the function height of image taking. Especially this second analysis is important by reason of the assessment of the atmosphere impact, and the accuracy of the correction.

5. Results and discussion

At the outset, the analysis of the homogeneous areas was performed on the images obtained at the flight altitudes. The analysis of brightness intensity of selected pixels of raw image (Fig. 4), located within the markers placed on the test areas (aluminium sheets arranged in the shape of a cross) indicated pixel brightness reduction together with the flight level, regardless of the recording channel. For higher flight levels, this is related to the small size of the markers themselves and averaging the reflection from their surface with the surrounding terrain. Marker values were recorded as 8 bits in the range from 0 to 255.

In individual raw image channels (Table 1), considerable differences were observed between the results for the visible and infrared channels. The values in the infrared channels were much lower, which resulted directly from the spectral nature of the markers used in the study.

The QUAC algorithm (Table 2) clearly reduced the brightness of pixels in the infrared channels, whereas in the case of visible channels the results were very similar to the raw data with a slight reduction of the atmospheric mist.

The situation was completely different in the case of the FLAASH algorithm (Fig. 6). The algorithm uses a model of separation of cirrus clouds, taking into account a special spectral channel in the range of 1360–1380 nm. The "cirrus" chan-
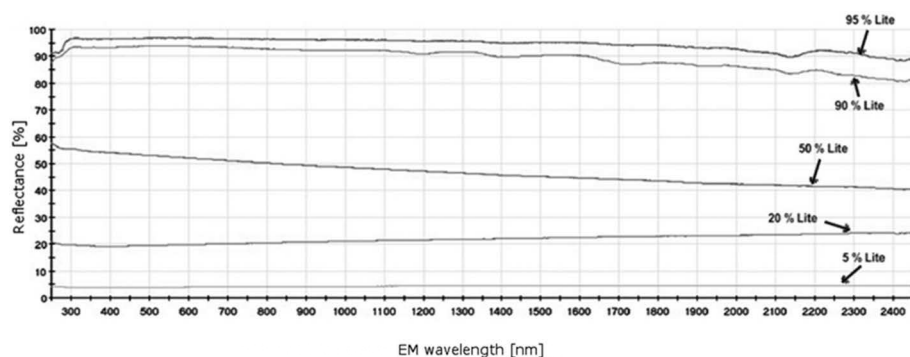

Figure 3. SphereOptics GmbH (2017) markers spectral curve

Table 1. Selected pixels intensity of RAW image with NDVI values

Altitude [m]	The central value of spectral range [nm]						NDVI [%]
	460	550	570	640	760	850	
300	255	255	255	255	137	103	-30.10
800	153	255	255	255	76	57	-54.08
1200	163	255	203	255	78	56	-53.15
1300	149	209	125	218	59	47	-57.40
1700	162	199	235	225	61	40	-57.34
2100	159	185	211	199	58	40	-54.86
2500	145	165	152	161	54	39	-49.77

Table 2. Selected pixels intensity QUAC algorithm processed image with NDVI values

Altitude [m]	The central value of spectral range [nm]						NDVI [%]
	460	550	570	640	760	850	
300	255	255	255	255	206	192	-10.63
800	175	255	255	255	166	143	-21.14
1200	183	255	199	255	151	120	-25.62
1300	209	205	115	216	108	101	-33.33
1700	132	197	222	233	130	94	-28.37
2100	146	175	205	194	80	72	-41.61
2500	130	152	139	152	45	31	-54.31

Table 3. Selected pixels intensity FLAASH algorithm processed image with NDVI values

Altitude [m]	The central value of spectral range [nm]						NDVI [%]
	460	550	570	640	760	850	
300	135	80	88	2	0	206	-100.00
800	0	120	130	44	182	144	61.06
1200	0	114	0	54	178	141	53.45
1300	0	14	0	0	138	118	100.00
1700	0	0	65	8	141	107	89.26
2100	0	0	14	0	136	102	100.00
2500	0	0	0	0	124	100	100.00

nel is available in Landsat 8 OLI scenes, and is not available for registration in typical aerial cameras. For low- and mid-range data, the FLAASH algorithm misidentifies the clouds. The algorithm classifies bright areas, including white patterns such as clouds and excludes them from classification (correction) by assigning high negative values to these pixels. As a result, these areas are "concealed". To illustrate the problem, the algorithm was used to correct all channel images acquired from seven different flight altitudes. The areas discussed are visible in the processed image as black spots. To quantify the results of the classification, the positive values obtained as a result of applying this correction method (the range 0–255) were recalculated and then the pixel values were read for the markers. The results are summarized in Table 3.

After the correction, it can be seen that the results obtained are clearly different from the source data. Only the pixels with small reflectance values are corrected properly, whereas bright pixels reach the values of 0 (the original values after the correction were expressed in the range from -32,768 to 0).

The analysis of the images before and after the correction clearly showed the difference between the results for both algorithms. The source image and resultant images are shown in Figures 4, 5 and 6.

Both the raw picture (Fig. 4) and the picture after QUAC correction (Fig. 5) are characterized by good contrast. The image after correction is slightly darker but still fully readable, which is the correct result of removing the effects of atmospheric scattering.

In the case of the image after correction with the FLAASH algorithm (Fig. 6), there are clearly visible black fields with the value 0, located in the brightest areas of the image. The interpretation potential of the image is reduced due to "concealing" of a part of the image area. In a cross-sectional perspective, it is worth analysing several graphs depicting a relationship between the raw image and post-correction image values using both algorithms.

For the 550, 570 and 640 nm channels (Figs. 7, 8 and 9), very high conformity was observed between the pixel values representing the markers on the raw image and after QUAC correction, while the values obtained after FLAASH correction were radically different.

In all the analysed cases, the image after correction (Fig. 7, 8 and 9) showed lower pixel values than those in the raw image. This indicates a correct reduction of a small (still increasing with flight altitude) brightening effect attributable to light scattering in the atmosphere. There is also a clear tendency to lower the brightness of the marker pixels as the flight altitude increases. This result seems inconsistent with the increasing share of the atmospheric mist; nonetheless, the cause lies in the relatively small size of the markers, which with the increasing flight altitude are represented by a smaller and smaller number

Figure 4. 640 nm optical band, altitude 1200 m, RAW image, scale on image 2

Figure 5. 640 nm optical band, altitude 1200 m, QUAC algorithm processed image, scale on image 2

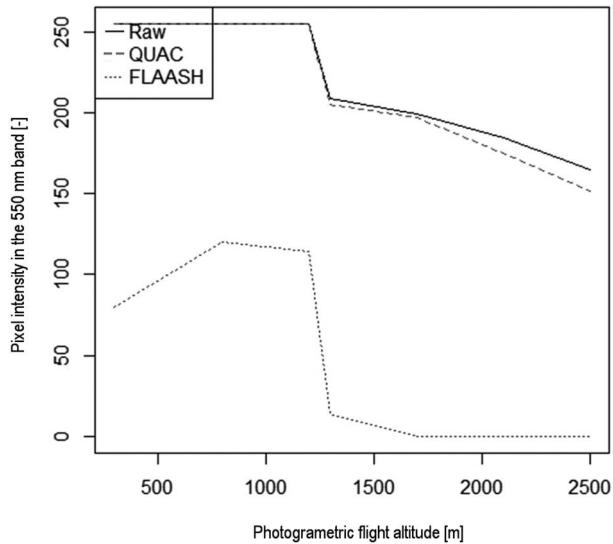**Figure. 640** nm optical band, altitude 1200 m, FLAASH algorithm processed image, scale on image 2

Figure 7. RAW image and processed images (QUAC, FLAASH) pixels intensities dependence for 550 nm optical band
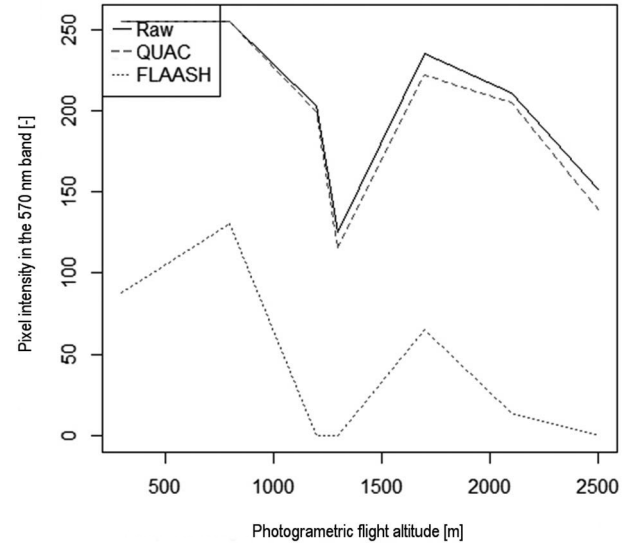

Figure 8. RAW image and processed images (QUAC, FLAASH) pixels intensities dependence for 570 nm optical band

of pixels. From a height of about 1700 m, the markers start to give the impression of being same as the surrounding area. At a height of 800 m GSD pixel represents a 0.25 m of a ground (the marker has the shape of a cross with dimensions of 2×2 m, and shoulder width 0.4 m). By reason of "concealing" considerable image areas when the FLAASH algorithm is used, for the quantitative analysis of the atmosphere impact, the results of the correction obtained by means of QUAC algorithm were used and related to the values of raw images in the form of a difference in value. The results are presented in Table 4.

In the case of absolute value analysis, particularly high differences for near-infrared channels are detectable. The algorithm caused a very clear image brightening.

The effects of the algorithm are evident in the table showing the percent correction of the image brightness (Table 4). It should be remembered that all the analyses presented above relate to the brightness level for the selected bright marker surfaces located in the studied area. If you analyse the whole image, the absolute and percent results will be different. However, they are not presented in the present paper.

An original method of estimating the atmosphere's influence on the values recorded in the picture

Comparable results were obtained using a proprietary software developed for the needs of the HESOFF project. The study area was established in the Forest District Karczma Borowa (coordinates of the area centre in the WGS84 system: 51.848766, 16.626985). In order to assess the impact of the atmosphere on the reflectance measurement in the au-
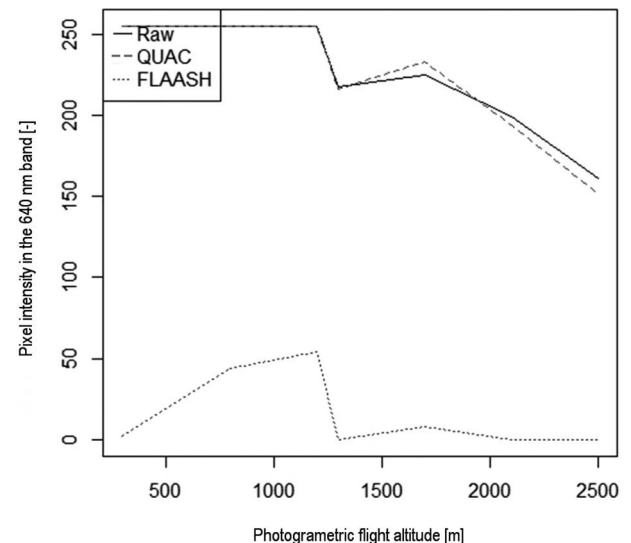

Figure 9. RAW image and processed images (QUAC, FLAASH) pixels intensities dependence for 640 nm optical band

tumn 2013, photographic missions were carried out over a forest area of 5 ha. A prototype multi-sensor platform Quercus 6, recording radiation in the ranges 635 and 865 nm, was used to acquire images. The computer program developed by the project team was used to analyse the images (Fig. 10). The reflectance was measured for the selected images of the same area made at different flight altitudes: 100 m, 400 m and 600 m. The result of the analysis is the graph showing the dependence of the reflectance on the flight altitude.

Table 4. The influence of atmospheric light scattering on pixels intensities (%)

Altitude [m]	The central value of spectral range [nm]					
	460	550	570	640	760	850
	[%]					
300	0.0	0.0	0.0	0.0	-50.4	-86.4
800	-14.4	0.0	0.0	0.0	-118.4	-150.9
1200	-12.3	0.0	2.0	0.0	-93.6	-114.3
1300	-40.3	1.9	8.0	0.9	-83.1	-114.9
1700	18.5	1.0	5.5	-3.6	-113.1	-135.0
2100	8.2	5.4	2.8	2.5	-37.9	-80.0
2500	10.3	7.9	8.6	5.6	16.7	20.5

6. Conclusion

The analysis of the results showed that the correlation of the recorded light intensity and the flight level is strongly positive, and the reflectance increases with altitude, both for red and infrared range. Even with a moderately low photogrammetric flight altitude, image brightness typical of satellite images was observed, which increased with flight altitude. This phenomenon is interpreted in three ways depending on the way of light scattering, that is, Rayleigh scattering, Mie scattering and non-selective scattering (Lillesand, Kiefer 1994). Rayleigh scattering occurs when radiation reacts with atoms and molecules, the size of which is much smaller than the wavelength. The oscillating electric field of a light wave acts on the charges within a particle, stimulates vibrations of electrons that emit photons of light. The effect associated with this phenomenon is inversely proportional to the fourth power of wavelength (Slater et al., 1983, Chavez 1988). It is worth noting that the molecules responsible for this phenomenon in the atmosphere over forest areas are the standard molecules that make up the atmosphere, that is, nitrogen, oxygen and so on, and gases typical of the forest ecosystem, that is, isoprene, monoterpenes, methanol and so on. The latter compounds, due to their size, scatter light with longer wavelengths. This type of scattering is homogeneous in all directions. It mainly concerns visible light. The second type of scattering (Mie scattering) occurs when the light wavelength is similar to the particle diameter. The phenomenon occurs mainly in the case of longer wavelengths. Typically water vapor and dust particles, and sometimes VOC particles, are examined with reference to Mie scattering. Mie scattering is inversely proportional to the wavelength (Slater et al. 1983). The third

type of scattering that was mainly observed in the present study is non-selective scattering. It occurs regardless of the wavelength of the light affecting particles with dimensions much larger than the wavelength (e.g., rain drops, 5–100 μm water vapor). Non-selective scattering is associated with visible, near and middle infrared light (Wołoszyn 2009).

If using the atmospheric correction algorithms for multispectral aerial images, the application of appropriate techniques of the correction should be considered in each case. On the one hand, available algorithms can be very simplified (QUAC), and bring about correct results only for representative scenes performed under standard conditions. Such algorithms are easy to use, but they are not suitable for images involving areas with atypical atmospheric components, for example, over the areas with rich vegetation. On the other hand, in the case of complex correction algorithms, there is a necessity to introduce a number of input parameters, the acquisition of which is impossible for typical aviation missions carried out for the needs of research projects. The lack of these parameters result in the erroneous classification of the areas recorded in the image, as it happens in the case of applying FLAASH correction (Figure 9). Additionally, it should be noted that in addition to the pixel brightness intensity, also remote sensing biomass indicators, such as EVI or NDVI, are sensitive to the flight level from which the measurement is made. For the examined pixels, the difference of the NDVI index ranged from 4.54% to 32.94% between images without and with the atmospheric correction. It should be remembered that with this type of indicators, image data from various optical channels are used. Between these, as demonstrated in this study, a significant variation in the atmosphere impact on the brightness level can be observed. In the case studied, for correction by the QUAC algorithm, the difference for 640 nm channel was quite small, and for 730 nm channel it

was significant. The solution to the problems identified may be further detailed in studies of theoretical and practical aspects of atmospheric correction for small areas. The works should take into account the nature of the studied area and effects of all atmosphere components pertinent to a given ecosystem.

Conflict of interest

The authors declare the lack of potential conflicts.

Acknowledgment and source of funding

References

ATCOR. 2015. http://www.rese.ch/products/atcor/index.html [30.05.2017].

Badawy B. 2011. Quantifying carbon processes of the terrestrial biosphere in a global atmospheric inversion based on atmospheric mixing ratio, remote sensing and meteorological data. Diss. Universität Jena. DOI 10.4126/98-004421237.

Burkart A., Aasen H., Alonso L., Menz G., Bareth G., Rascher U. 2015. Angular dependency of hyperspectral measurements over wheat characterized by a novel UAV based goniometer. *Remote Sensing* 7(1): 725–746. DOI 10.3390/rs70100725.

Campbell J.E., Shin M. 2012. Satellite Imagery and Aerial Photography, in: Geographic Information System Basics v. 1.0, 94–99. DOI 10.1016/0034-4257(88)90019-3.

Chavez P.S. 1988. An improved dark-object subtraction technique for atmospheric scattering correction of multispectral data. *Remote Sensing of Environment* 24: 459–479. DOI 10.1016/0034-4257(88)90019-3.

Czapski P., Kacprzak M., Korniluk T., Kotlarz J., Kubiak K., Mazur A., Mrowiec K., Oszako T., Pieniążek J., Pośpieszczyk A., Tkaczyk M., Wodziński K., Zalewska N. 2014. Budowa i zastosowanie platformy wielosensorowej w badaniu wybranych parametrów środowiska. *Prace Instytutu Lotnictwa* 1(234): 126–142. DOI 10.15199/50.2016.3.1.

Delwiche C.F., Sharkey T.D. 1993. Rapid appearance of 13C in biogenic isoprene when 13CO2is fed to intact leaves. *Plant, Cell and Environment* 16: 587–591.

Fall R., Benson A.A. 1996. Leaf methanol-the simplest natural product from plants. *Trends in Plant Sciences* 1: 296–301. DOI 10.1016/S1360-1385(96)88175-0.

Fall R. 2003. Abundant oxygenates in the atmosphere: A biochemical perspective. *Chemical Reviews* 103: 4941–4495. DOI 10.1021/cr0206521.

Fuentes J.D., Lerdau M., Atkinson R., Baldocchi D., Bottenheim J.W., Ciccioli P., Lamb B., Geron C., Gu L., Guenther A., Sharkey T.D., Stockwell W. 2000. Biogenic hydrocarbons in the atmospheric boundary layer: A review. *Bulletin of the American Meteorological Society* 81: 1537–1575. DOI 10.1175/1520-0477(2000)081.

Głowienka E. 2008. Porównanie metod korekcji atmosferycznej dla danych z sensorów hiperspektralnych 18, Akademia Górniczo-Hutnicza w Krakowie, Katedra Geoinformacji, Fotogrametrii i Teledetekcji Środowiska. Archiwum Fotogrametrii, Kartografii i Teledetekcji, Kraków. ISBN 978-83-61576-08-2.

Guenther A., Hewitt C.N., Erickson D., Fall R., Geron C., Graedel T., Harley P., Klinger L., Lerdau M., McKay W.A., Pierce T., Scholes B., Steinbrecher R., Tallamraju R., Taylor J., Zimmerman P. 1995. A global model of natural volatile organic compound emissions. *Journal of Geophysical Researcg: Atmospheres* 100: 8873–8892. DOI 10.1029/94JD02950.

Guenther A., Zimmerman P., Wildermuth M. 1994. Natural volatile organic compound emission rates for U.S. woodland landscapes. *Atmospheric Environment* 28: 1197–1210. DOI 10.1016/1352-2310(94)90297-6.

Houghton R.A., Nassikas A.A. 2017. Negative emissions from stopping deforestation and forest degradation, globally. *Global Change Biology* 24(1): 350–359. DOI 10.1111/gcb.13876.

Jardine K., Harley P., Karl T., Guenther A., Lerdau M., Mak J.E. 2008. Plant physiological and environmental controls over the exchange of acetaldehyde between forest canopies and the atmosphere. *Biogeosciences* 5: 1726–4170. DOI 10.5194/bg-5-1559-2008.

Jarocińska A. 2012, Zastosowanie modeli transferu promieniowania w hiperspektralnych badaniach stanu roślinności łąk. Uniwersytet Warszawski, Wydział Geografii i Studiów Regionalnych, rozprawa doktorska.

Kaneko E., Aoki H., Tsukada M. 2016. Image-based path radiance estimation guided by physical model. Geoscience and Remote Sensing Symposium (IGARSS), IEEE International. DOI 10.1109/IGARSS.2016.7730811.

Khodri M., Swingedouw D., Mignot J., Sicre M.-A., Garnier E., Masson-Delmotte V., Ribes A., Terray L. 2017. Klimat ostatniego tysiąclecia. *Przegląd Geofizyczny* 58(1-2): 55–82. DOI 10.4267/2042/56360.

Kiendler-Scharr A., Wildt J., Dal Maso M., Hohaus T., Kleist E., Mentel T.F., Tillmann R., Uerlings R., Schurr U., Wahner A. 2009. New particle formation in forests inhibited by isoprene emissions. *Nature* 461: 381–384. DOI 10.1038/nature08292.

Kotula A. 2011. Czynniki kształtujące jakość radiometryczną ortofotomapy w procesie fotogrametrycznym. Akademia Górniczo-Hutnicza im. Stanisława Staszica w Krakowie, Wydział Geodezji Górniczej i Inżynierii Środowiska Katedra Geoinfromatyki, Fotogrametrii i Teledetekcji, Kraków.

Lillesand T.M., Kiefer R.W. 1994. Remote Sensing and Photo Interpretation, 3rd. ed. John Wiley& Sons, New York, 750 p. ISBN 3540528059.

MODTRAN. 2016. http://modtran5.com/about/index.html [12.10.2016].

Niinemets U., Loreto F., Reichstein M. 2004. Physiological and physico-chemical controls on foliar volatile organic compound emissions. *Trends in Plant Sciences* 9: 180–186. DOI 10.1016/j.tplants.2004.02.006.

Ochtyra A., Zagajewski B., Kozłowska A., Marcinkowska-Ochtyra A., Jarocińska A. 2016. Ocena kondycji drzewostanów Tatrzańskiego Parku Narodowego za pomocą metody drzewa decyzyjnego oraz wielospektralnych obrazów satelitarnych Landsat 5 TM. *Sylwan* 160(3): 256–264.

Osińska-Skotak K. 2005. Wpływ korekcji atmosferycznej na wyniki cyfrowej klasyfikacji. *Acta Sciennarum Polonorum: Geodesia et Descriptio Terrarum* 4(1): 41–53.

Osińska-Skotak K. 2007. Znaczenie korekcji radiometrycznej w procesie przetwarzania zdjęć satelitarnych. Archiwum Fotogrametrii, Kartografii i Teledetekcji 17b, Wydział Geodezji i Kartografii, Politechnika Warszawska. ISBN 978-83-920594-9-2.

Shu Y., Atkinson R. 1995. Atmospheric lifetimes and fates of a series of sesquiterpenes. *Journal of Geophysical Research* 100: 7275–7281. DOI 10.1029/95JD00368.

Slater P., Doyle F., Fritz L., Welch R. 1983. Photographic systems for remote sensing. *American Society of Photogrammetry Second Edition of Manual of Remote Sensing* 1(6): 231–291. ISBN 0686231082.

Song C., Woodcock C.E., Seto K.C., Lenney M.P., Macomber S.A. 2001. Classification and Change Detection Using Landsat TM Data: When and How to Correct Atmospheric Effects? *Remote Sensing of Environment* 75: 230–244. DOI 10.1016/S0034-4257(00)00169-3.

SphereOptics 2017. Herrsching, Germany, http://sphereoptics.de/en/contact/adress-and-technical-contact-persons/ [30.11.2017].

Tellidis I., Levin E. 2014. Photogrammetric Image Acquisition with Small Unmanned Aerial Systems. ASPRS Annual Conference Louisville, Kentucky, 23–28.

Trainer M., Williams E.J., Parrish D.D., Buhr M.P., Allwine E.J. 1987. Models and observations of the impact of natural hydrocarbons on rural ozone. *Nature* 329: 705–707. DOI 10.1038/329705a0.

Warneke C., Karl T., Judmaier H., Hansel A., Jordan A., Lindinger W. 1999. Acetone, methanol, and other partially oxidized volatile organic emissions from dead plant matter by abiological processes: Significance for atmospheric HOx chemistry. *Global Biogeochemical Cycles* 13: 9–17. DOI 10.1029/98GB02428.

Wołoszyn E. 2009. Meteorologia i klimatologia w zarysie. Wydawnictwo Politechniki Gdańskiej, Gdańsk. ISBN 978-83-7775-237-1.

Authors contribution

A.M. – organization of photogrammetric flights, data post-processing, analysis of reflectance curves, manuscript writing; M.K. – photogrammetric coating, spectral curves analysis, photogrammetric analysis, manuscript correction/revision; K.K. – analysis of spectral reflectance curves, manuscript correction/revision; J.K. – preparation of software for data post-processing, manuscript correction/revision; K.S. – processing of spectral data using the QUAC and FLAASH algorithms, manuscript correction/revision.

Translated by: Bożena Kornatowska